ACS APPLIED MATERIALS & INTERFACES

Research Article

www.acsami.org

Dimensional and Structural Control of Silica Aerogel Membranes for Miniaturized Motionless Gas Pumps

Shanyu Zhao,[†] Bo Jiang,*[,‡] Thomas Maeder,[‡] Paul Muralt,[‡] Nayoung Kim,[†] Santhosh Kumar Matam,[†] Eunho Jeong,[†] Yen-Lin Han,[§] and Matthias M. Koebel*[,†]

[†]EMPA, Swiss Federal Laboratories for Materials Science and Technology, CH-8600 Dübendorf, Switzerland

[‡]EPFL, Swiss Federal Institute of Technology Lausanne, CH-1015 Lausanne, Switzerland

[§]Seattle University, Seattle, Washington 98122, United States

Supporting Information

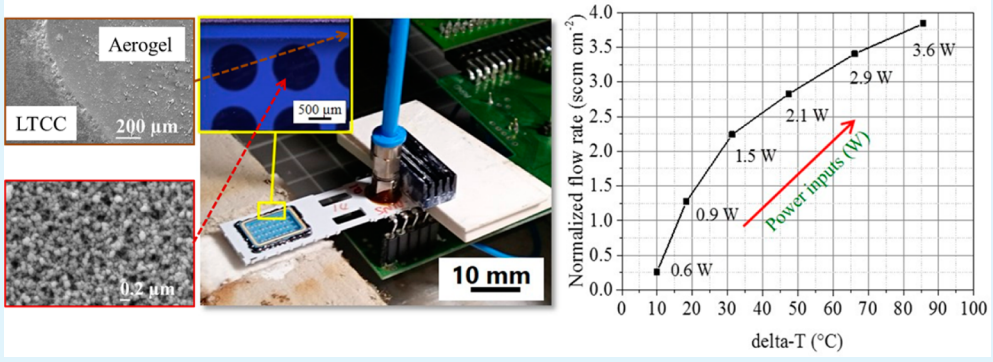

ABSTRACT: With growing public interest in portable electronics such as micro fuel cells, micro gas total analysis systems, and portable medical devices, the need for miniaturized air pumps with minimal electrical power consumption is on the rise. Thus, the development and downsizing of next-generation thermal transpiration gas pumps has been investigated intensively during the last decades. Such a system relies on a mesoporous membrane that generates a thermomolecular pressure gradient under the action of an applied temperature bias. However, the development of highly miniaturized active membrane materials with tailored porosity and optimized pumping performance remains a major challenge. Here we report a systematic study on the manufacturing of aerogel membranes using an optimized, minimal-shrinkage sol–gel process, leading to low thermal conductivity and high air conductance. This combination of properties results in superior performance for miniaturized thermomolecular air pump applications. The engineering of such aerogel membranes, which implies pore structure control and chemical surface modification, requires both chemical processing know-how and a detailed understanding of the influence of the material properties on the spatial flow rate density. Optimal pumping performance was found for devices with integrated membranes with a density of 0.062 g cm^{-3} and an average pore size of 142.0 nm. Benchmarking of such low-density hydrophobic active aerogel membranes gave an air flow rate density of 3.85 sccm·cm^{-2} at an operating temperature of 400 °C. Such a silica aerogel membrane based system has shown more than 50% higher pumping performance when compared to conventional transpiration pump membrane materials as well as the ability to withstand higher operating temperatures (up to 440 °C). This study highlights new perspectives for the development of miniaturized thermal transpiration air pumps while offering insights into the fundamentals of molecular pumping in three-dimensional open-mesoporous materials.

KEYWORDS: *aerogel membrane, miniaturized gas pump, sodium silicate, low-temperature cofired ceramics, Knudsen flow*

INTRODUCTION

Advances in microeletromechanical systems (MEMS) have sparked considerable interest in miniaturizing thermal and/or chemical systems for portable medical devices, gas analysis, global positioning systems, fuel cells and microcombustion devices in portable unmanned vehicles, etc.[1,23−56] These systems commonly require gas pumps for forced convection, gas supply, and sampling or vacuum operation. Conventional miniaturized pumps are commonly based on the diaphragm displacement principle with moving parts, which are difficult to realize and operate efficiently due to mechanical friction losses, size scaling effects, manufacturing tolerances, and issues with packaging.[7] Thermal transpiration pumps maintain a certain pressure gradient commonly referred to as the thermomolecular pressure difference as a consequence of thermal excitation of gas molecules in a low-dimensional system. The absence of

Received: June 19, 2015
Accepted: August 5, 2015
Published: August 5, 2015

DOI: 10.1021/acsami.5b05462
ACS Appl. Mater. Interfaces 2015, 7, 18803−18814

moving parts represents a conceptual advantage for cost-effective long-lifetime miniaturized gas pump development efforts.[8] Among these thermal transpiration pumps, Knudsen pumps leverage the thermal transpiration phenomenon of a rarefied gas and are operated by using high porosity, low thermal conductivity transpiration membranes under the action of a temperature gradient.[9] Muntz and co-workers have developed a validated model for single- and multiple-stage Knudsen compressors.[10−13] It states that the mass flow rate $\dot{M}$ of a gas with a molecular mass m, through a membrane comprising channels of a length L_x and a pore radius L_r with a total cross-sectional area A, can be written for straight capillary channels and small temperature and pressure gradients as[10,14]

$$\dot{M} = P_{avg}\sqrt{\frac{m}{2kT_{avg}}}\left(\frac{L_r}{L_x}A\right)\left(\frac{\Delta T}{T_{avg}}Q_T - \frac{\Delta P}{P_{avg}}Q_P\right) \quad (1)$$

For a transitional flow through long circular capillary tubes, the flow coefficients Q_T for the thermally driven flow and Q_p for the pressure driven flow can be derived from the linearized Boltzmann equations.[12,15] The ideal pumping efficiency of a Knudsen pump without considering thermal losses is given as[16]

$$\eta_{ideal} = \frac{R}{C_P}\left(\frac{\sqrt{T_{hot}/T_{cold}} - P_{hot}/P_{cold}}{P_{hot}/P_{cold} + \sqrt{T_{hot}/T_{cold}}}\right) \quad (2)$$

Aerogels are ideal candidate materials for constructing such membranes because (i) they feature very low skeletal and gas thermal conductivities, giving rise to an ultralow overall thermal conductivity in the range of 0.012−0.020 W m^{-1} K^{-1} at 25 °C/1 atm in the case of silica-based aerogels,[17] which is essential for the overall efficiency of the device and (ii) the material consists of a solid open-porous structure with a typical average pore size in the 10−100 nm range that is comparable to the mean free path of air molecules required for obtaining rarefied air flow conditions.[18] Aerogel materials can be made of silica,[19−24] carbon,[25−28] organic derived compounds[29−31] or other mineral type oxides.[32,33] From this list, silica-based aerogels show a unique combination of features such as high temperature resistance,[34] simple fabrication processes already scaled to industrial volumes[35,36] as well as straightforward functionalization (i.e., through nanodoping, addition of IR opacifiers, or catalytically active species).[37−40] In addition, the pore size distribution, surface structure as well as physicochemical properties of silica aerogels can be readily tailored as they are the most studied and best documented class of aerogels.[41−44]

The use of silica aerogel based membranes for micro-Knudsen pumps (μ-KPs) has been reported previously: Han et al.[45,46] have demonstrated a mesoscale cascade staged Knudsen pump using carbon doped silica aerogel membranes for low pressure air compression. The 15-stage cascade device has produced a maximum differential pressure of 150 mbar but no information on flow rate was reported in their work. According to their findings, the pumping performance is determined by the magnitude of the steady state temperature bias acting across the membrane, which is directly linked to the thermal insulation properties of the membrane as well as its pore structure. Ochoa and Ronney[47] have proposed a self-pumping concept for mesoscale combustors, where the heat of combustion is utilized for air pumping in an μ-KP component made of commercial silica aerogel. The miniaturized pump prototype with a diameter of 12 mm and a thickness of 4 mm was able to deliver a gas flow rate of 2 mL min^{-1} with a differential pressure of 60 mbar at an active temperature bias of 150 °C. However, most studies in the field of μ-KPs focus on device prototyping, often utilizing commercial silica aerogel materials. To date there is a lack of R&D developments targeting the fabrication of suitable aerogel membranes. To the best of our knowledge, there is no prior investigation that aims to elucidate the influence of the silica aerogel structure and surface chemistry on the pumping efficiency of μ-KPs. Since very little systematic work has been published in this field, a large amount of development work in pore structure engineering and system integration is still required in order to accomplish the full potential of miniaturized Knudsen gas pumps. From a materials synthesis point of view, many process parameters directly affect the mesoporous aerogel network structures: among the best-known structure directing parameters in aerogel synthesis are precursor type and concentration,[48,49] catalyst type and concentration,[50−52] as well as gelation, aging, and processing conditions.[51]

In this work, we describe a novel and simple silica aerogel membrane fabrication method capable of delivering a wide range of aerogel membrane microstructures by varying the synthesis parameters. A μ-KP testing demonstrator was constructed to characterize the pumping performance of the integrated aerogel membranes. For the first time, this work provides physical and chemical insights into how the structural and chemical aerogel properties affect the μ-KP pumping performance as well as on the thermal transpiration pump mechanism for aerogel materials.

Using our proposed synthesis procedure, pristine silica aerogel membranes of 0.6−0.7 mm thickness can be directly synthesized inside a microfabricated ceramic mold produced by Low-Temperature Co-fired Ceramic technology (LTCC). Due to its fragility and brittleness, it is challenging to machine silica aerogels into a microscale membrane of precisely defined shape which is needed for a μ-KP application.[53] Therefore, we have developed a micromold casting method to synthesize silica aerogel inside the LTCC mold, eliminating the problematic machining and affixing (gluing) steps. A minimal shrinkage processing route is needed to extend the use of silica aerogels to membranes for μ-KP applications. Sol−gel casting of aerogel membranes and subsequent processing steps were evaluated for two types of silica precursor chemistries namely tetraethyl orthosilicate (TEOS) and silicic acid (ion exchanged sodium silicate) in an attempt to develop crack-free, low-shrinkage silica aerogel membrane module prototypes. Subsequently, membrane modules were manufactured with varied pore structure by tuning the silica content in the sol from (5−10% in terms of SiO_2 equivalent mass loading) and the surface chemical characteristics through postmodification with hydrophobic trimethylsilyl groups.

EXPERIMENTAL SECTION

Materials and Chemicals. Sodium silicate solution (26.5% w/w SiO_2 in water, Na_2O:SiO_2 molar ratio = 1:3.1) obtained from Sigma-Aldrich, and research grade PEDS, a prepolymerized form of tetraethoxysilane (TEOS) containing a water-to-TEOS molar ratio of 1.5 and a SiO_2 content of 20% w/w in ethanol (PEDS-P75E20, PCAS, France, colloidal size distribution is shown in Figure S1a), were used as silica gel precursors. Hexamethyldisilazane (HMDZ, 98.5%, ABCR GmbH & Co., Germany), hexamethyldisiloxane (HMDSO, ≥ 98.5%, Sigma-Aldrich, Switzerland) and trimethylchlorosilane (TMCS, ≥ 98%, Sigma-Aldrich, Switzerland), were used as hydrophobizing agents. Ethanol (F25-AF-MEK ethanol denatured with 2% methyl ethyl ketone, Alcosuisse, Switzerland) was used as a gelation solvent.

DOI: 10.1021/acsami.5b05462
ACS Appl. Mater. Interfaces 2015, 7, 18803−18814

Scheme 1. Fabrication of Sodium Silicate-Based Aerogel Membranes in LTCC Molds, (a) Casting of the Activated Silica sol into the LTCC Mold; (b) Moving the Submerged LTCC Mold around within the Container to Get Rid of Air Bubbles; (c) Placing a PS Lid with Holes on Its Side onto the Mold to Control the Thickness of the Membrane and Create a Flat Gel Surface Followed by Aging of the Gel for 24 h at Ambient Temperature; (d) Removing Excessive Hydrogel and Exchanging the Pore Fluid of the Gel; (e) Removing the Lid and Transferring the Membrane into a Glass Beaker; (f) Carrying out Ethanol Exchange and a Subsequent Surface Modification; (g) Drying of the Membranes in Supercritical CO_2

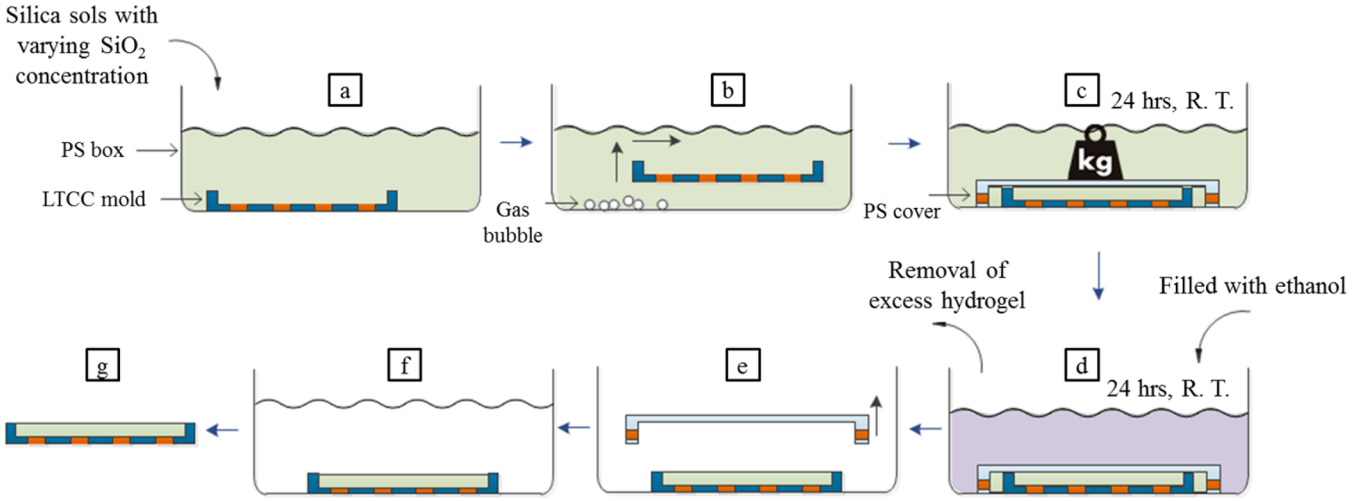

Table 1. Volumetric Mass Density, Linear Shrinkage, BET Specific Surface Area, Pore Volume, and Average Pore Diameter of Silica Aerogels

samples	SiO_2 content in the sol (% w/w)	bulk density (g cm^{-3})	skeletal density (g cm^{-3})	BET surface area (m^2 g^{-1})	BJH desorption cumulative pore volume V'_{pore} (cm^3 g^{-1})	BJH desorption pore diameter D'_{pore} (nm)	calcd[a] V_{pore} (cm^3 g^{-1})	calcd[a] D_{pore} (nm)	porosity[a] (%)	Knudsen number from D_{pore}, K_n[b]
SA-5-U	5	0.070 ± 0.002	2.116 ± 0.028	597	3.8	13.6	13.8	92.6	97	1.4
SA-5-M	5	0.062 ± 0.003	2.120 ± 0.031	441	3.1	14.1	15.7	142.0	97	1.0
SA-7.8-M	7.8	0.110 ± 0.006	2.118 ± 0.013	583	4.5	18.2	8.6	59.1	95	2.4
SA-10-M	10.0	0.130 ± 0.002	2.116 ± 0.073	782	3.6	11.4	7.2	36.9	94	3.8

[a]See eqs S2–S4. [b]K_n is calculated on the basis of the ratio of air molecular mean free path to the characteristic length of the membrane (pore size), where the air molecular mean free path is considered at ambient atmosphere and an average temperature in the aerogel membrane, with the hot side at T_{hot} = 400 °C and cold side at T_{cold} = 310 °C.

Hydrochloric acid (HCl, 37%) and ammonium hydroxide solution ($NH_3{\cdot}H_2O$, 28–30%) were purchased from Sigma-Aldrich (Switzerland). Deionized water was used in all experiments. All chemicals were used as received without any further purification.

SiO_2 Aerogel Membrane Synthesis. A dilute sodium silicate solution was prepared (containing ~10% w/w SiO_2) by mixing 1 part of concentrated sodium silicate solution with 2 parts of deionized water. This solution was passed through a cationic ion-exchange resin (Amberlite, IR-120H, Sigma-Aldrich) filled packed bed column. The resulting aqueous silica sol has a pH in the range of 2.2–2.5 (826 pH mobile, Metrohm Schweiz AG, Switzerland). A final adjustment of the silica concentration in the sol was carried out by diluting the 10% w/w silica solution to 7.8% w/w and 5% w/w with the required amounts of deionized water, respectively. The gelation was triggered by addition of a NH_4OH (2.5 M) solution to reach a pH of 5–6. The activated silica sol was cast into the LTCC mold and the submerged LTCC mold was agitated to eliminate air bubbles. A polystyrene (PS) lid with holes was placed onto the mold to control the thickness of the membrane and to create a flat gel surface. Gelation occurred in approximately 8–10 min at room temperature (RT, ~25 °C) after which the wet gels were aged for 24 h at RT. The general synthesis and casting scheme is shown in Scheme 1.

Solvent exchange of the gels into ethanol at RT resulted in a slight shrinkage, primarily observed on the top of the gels (a slight anisotropy arises because of the different contacting interfaces at the top and bottom respectively, LTCC (bottom) and PS (top)), which allowed the membranes to be easily removed from the PS box (shown in Scheme 1e) and placed in glass beaker filled with ethanol and covered with aluminum foil. The gel membranes were washed with ethanol two more times at 55 °C. Chemical modification of the gel's inner surfaces was carried out by soaking them in a dilute solution of hexamethyldisilazane in ethanol with an EtOH/HMDZ molar ratio of 17:1 at 65 °C for 24 h. Finally, the gel membranes were placed inside an autoclave and the hydrophobization solution pore fluid replaced by liquid CO_2 in a SCF extractor (Autoclave 4334/A21–1, Separex, France) over the course of 12h. The gels were then supercritically dried from carbon dioxide (CO_2) to yield the final monolithic aerogel membranes.

Integration of Silica Aerogel Membranes. To characterize the Knudsen pumping performance of the aerogel membranes, an LTCC-based testing device was developed in parallel. The device is based on a mesosacle LTCC fabricated substrate with embedded platinum resistive heaters as well as gas fluidic channels. Such an LTCC hot plate can easily reach temperatures above 400 °C in its heating region (hot zone namely), providing the thermal energy needed for the thermal-transpirationn pumping action, while the unheating region (cold zone namely) on the same device can be kept at a temperature below 100 °C when actively cooled.[54] Additionally, the embedded fluidic channels, which were prepared according to previously reported LTCC fine structuration methods,[55] were used for transporting the pumped air from the aerogel membrane to an external outlet through the hot plate for the flow rate measurement (AWM3000 Honeywell). The pressure drop of the flow due to the fluidic channel in the hot plate and the external tubing was estimated to be less than 1 Pa and

DOI: 10.1021/acsami.5b05462
ACS Appl. Mater. Interfaces 2015, 7, 18803–18814

will not be considered in the air flow rate measurement. The LTCC mold which the silica aerogel was cast into was sealed onto the device using glass frit sealing materials through firing at 400 °C for 4 min with a ramp rate of 5 °C/min. More information on the design and fabrication of the μ-KP devices will be reported in a future publication and will not be discussed here in detail.

SEM Characterization. Silica aerogel membranes were analyzed by fixing the samples on a sample holder using a sticky carbon pad, followed by coating them with a 10 nm thick platinum layer. SEM analysis of all materials was performed on a FEI Nova NanoSEM 230 instrument (FEI, Hillsboro, Oregon, USA) at an accelerating voltage of 10 kV and a working distance of 5 mm.

Evaluation of Density and Porosity. The bulk density was determined from the envelope volume, determined by the powder displacement method (GeoPyc 1360, Micromeritics, US) and the skeletal density was obtained from the skeletal volume, determined by helium pycnometry (AccuPyc II 1340, Micromeritics, US) (see Table 1). Porosities were calculated according to eq S2.

Evaluation of the Brunauer–Emmett–Teller (BET) Specific Surface Area. Nitrogen adsorption and desorption isotherms at −196 °C were obtained on a Micromeritics ASAP 2020c instrument with 15 s equilibration time. The specific surface area of the samples was determined by the Brunauer–Emmett–Teller (BET) method. The pore size distributions and pore diameter D'_{pore} were obtained from the desorption branch of the isotherm using the Barrett–Joyner–Halender (BJH) model.[56]

Evaluation of the Pore Volume, Pore Diameter of Silica Aerogels Membranes. The pore volume (V_{pore}), average pore diameter (D_{pore}), and porosity of the aerogels were calculated from the envelope and skeletal densities of the aerogel and their specific surface area using eqs S3 and S4.

Evaluation of the Thermal Conductivity. Thermal conductivities were determined from separately prepared square plate specimens (around 48 × 48 × 7 mm^3, cast simultaneously from the same sols) of monolithic aerogels using a custom built guarded hot plate device (guarded zone: 50 × 50 mm^2, measuring zone: 25 × 25 mm^2) designed for small samples of low thermal conductivity materials with a 15 °C temperature difference.[57] To be consistent with measurements according to European Standards,[57] we carried out calibration measurements using conventional expanded polystyrene samples measured once in a 50 × 50 cm^2 calibrated and validated testing equipment. The small guarded hot plate measurement data were then calibrated using these known standards.

Evaluation of the Thermal Stability. Differential thermogravimetric analysis was conducted on a TGA7 analyzer (PerkinElmer, USA) with the aim to identify the onset temperature to the degradation/loss of hydrophobic TMS groups which represents an upper boundary for operation temperature.

Fourier Transform Infrared Spectroscopy (FTIR). FTIR spectroscopy was carried out on a Bruker Tensor 27 spectrometer. Samples were analyzed in attenuated total reflectance mode (ATR) using a Pike MIRacle accessory equipped with a diamond crystal. The spectrum was collected 32 times and corrected for background noise.

Evaluation of the Contact Angle. The surface wettability of silica aerogel membranes was evaluated by contact angle measurement, using a Contact Angle System OCA (Dataphysics TBU 90E, Germany), combined with a high-speed camera. Water droplets were deposited directly at the top or bottom surfaces of the dried material, the water contact angles (WCAs) were measured. Three measurements were performed per sample and averaged. The volume of the water droplet was 5 μL, and the tip used was a precision stainless steel tip (Gauge 32, EFD).

RESULTS AND DISCUSSION

Aerogel Membrane by the Direct Microsized Casting. The preparation of thin aerogel membranes for μ-KPs with high shape fidelity and ultralow shrinkage is an ambitious endeavor. Because bulk aerogel materials made from silica are very brittle, subtractive methods are ill-suited to prepare form parts as they can easily damage the membrane for example during machining.[47] The direct form casting of aerogel membranes into a suitable mold on the other hand is a promising approach, particularly for small specimen sizes. However, this methodology requires great care and the development of customized gelation and postprocessing methods since gel shrinkage results in a dimensional mismatch which leads to cracks along the aerogel/mold interface which can cause device failure due to a short-circuit air conduction pathway. We therefore developed a minimal shrinkage procedure to directly prepare aerogel membranes inside the 9 mm × 6 mm × 0.75 mm cavity of the LTCC molds.

Several synthesis parameters critically affect shrinkage and/or deformation of the aerogel membranes: the sol–gel chemical system itself, the sol-casting and gelation procedure, the solvent exchange steps, and most critically, the drying step.[58]

First, the type of silica sol precursor chemistry used has a strong influence on the stability (e.g., shrinkage, deformation and spring-back effect) of the resulting gel membrane during aging and processing. We have compared TEOS and sodium silicate aerogels (over a 5–10% w/w silica concentration range in the respective sols). The silica sol concentration primarily determines density and pore diameter of the aerogel materials. The range of accessible pore sizes is limited because of (i) the technological challenges to synthesize ultralow density aerogel materials ($\rho_{bulk} \leq 0.05$ g/cm^3) and (ii) the rapidly deteriorating efficiency of the μ-KP system with increasing membrane density (decrease in the respective mesopore sizes) when using more concentrated silica sols.[59] It was found that the TEOS-based aerogels synthesized in an ethanol-based solvent system resulted in more pronounced dimensional changes (shrinkage and springback) during aging and silylation treatments (see Figure S2), making high-quality mold casting almost impossible. Further characterization results of the TEOS based aerogels are shown in Figure S3. In comparison, ion exchanged sodium silicate based gels proved much more dimensionally stable during the LTCC mold casting and processing. According to the literature,[60] the shrinkage of the gels derived from different precursors most probably due to the nanostructuration of the resulting gels, which may be affected, in this study, by the colloidal particle size and distribution of the prepolymerized silica sols (PEDS and silicic acid), shown in Figure S1, and it eventually leads to a variation of primary particles size, pores size distribution, fractality, tortuosity etc. of the aerogel materials.

Second, the type of surface modification treatment was chosen to induce the smallest possible stresses and dimensional changes in the wet gels. Three common silylation agents (HMDSO, HMDZ and TMCS) have been tested. HMDZ-modified aerogel membranes displayed the highest shape fidelity, which is consistent with the literature.[61]

Furthermore, a very low viscosity silica sol must be employed for sol-casting in order to minimize the gas–liquid interfacial tension and thus to prevent the introduction and trapping of air bubbles during mold casting. Here, it was found that a 2 min centrifugation of the sol at 3000 rpm just after base addition and before casting followed by the direct immersion of the LTCC mold in the sol effectively avoids the formation of gas bubble defects in the membranes.

Furthermore, drying also plays a critical role in replicating crack-free aerogel membranes. Typically aerogels can be dried in three different ways namely (i) ambient pressure drying from a low-surface tension organic solvent, (ii) freeze-drying and (iii)

DOI: 10.1021/acsami.5b05462
ACS Appl. Mater. Interfaces 2015, 7, 18803–18814

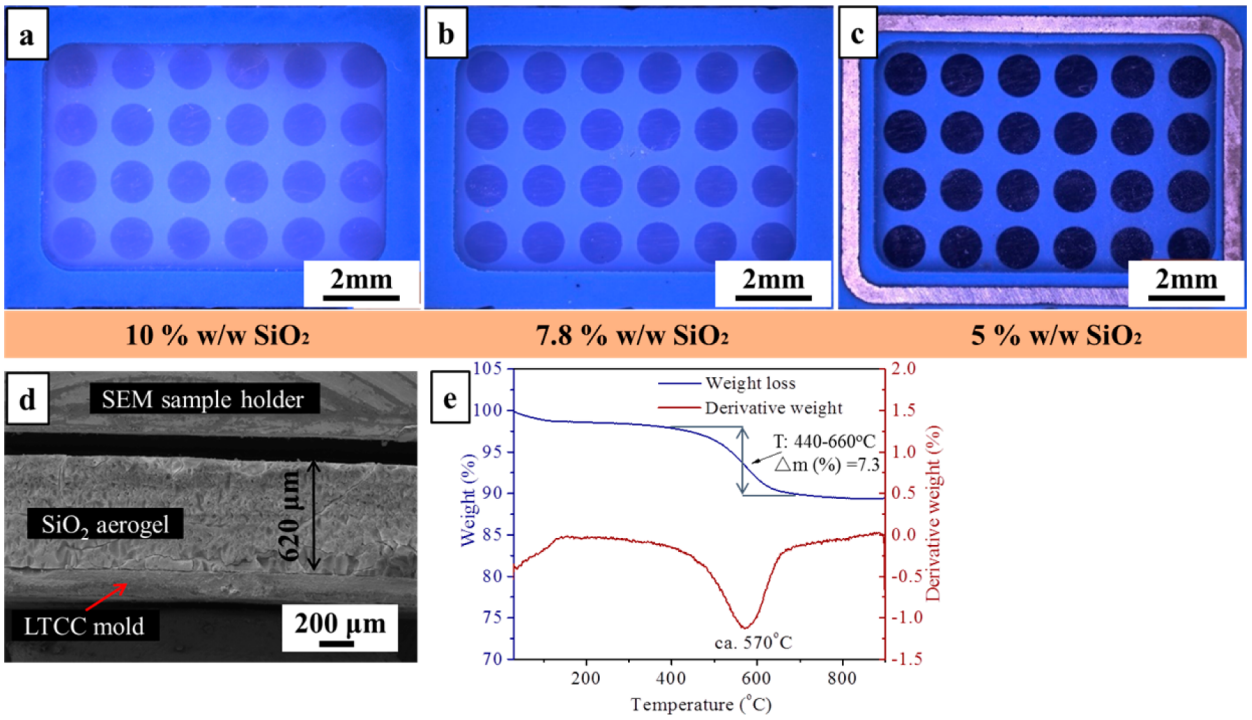

Figure 1. Silica aerogel membranes embedded in Alumina LTCC molds prepared with (a) 10% SiO_2, SA-10-M; (b) 7.8% SiO_2, SA-7.8-M; and (c) 5% SiO_2, SA-5-M; (d) SEM images of the thickness of the membrane of SA-5-M; (e) thermogravimetric analysis of the aerogel material on SA-5-M membrane.

drying from supercritical fluids (CO_2, alcohols, acetone etc.).[60] Supercritical drying (commonly from CO_2) exerts the smallest mechanical stresses on the particle network structure and yields the highest quality (crack free) dry aerogels with minimal shrinkage. Therefore, it was the method of choice for this study where shrinkage and cracking need to be avoided at all cost.[62]

With the help of the above-mentioned optimized procedure, we were able to cast silica aerogel membranes just a few hundred micrometerss thick. The high shape fidelity, particularly along the LTCC/aerogel interfaces, of the so-prepared membranes can be clearly seen in the photographic images, (Figure 1). By changing the silica concentration and surface modification treatment, aerogel membranes with a range of pore sizes and surface chemical properties were prepared and tested on a miniaturized μ-KP system. An overview of the different samples and their physical properties is given in Table 1.

Structural and Thermal Properties of Silica Aerogel Membranes and Their Performance in Miniaturized Model Knudsen Pump Devices. According to the Muntz model (eq 1), there are three main factors which determine the effectiveness of a thermal transpiration membrane, namely (i) the channel size needed to operate in a given Knudsen number range, (ii) a high gas conductance which is directly linked to the porosity and pore size distribution, and (iii) a low thermal conductivity which minimizes skeletal conduction losses through the membrane struts. Accordingly, the following materials and system design parameters must be taken into account when attempting to maximize μ-KP performance:[59] the thickness of the membrane L_x, the membrane thermal transpiration area A, the membranes pore radius D_γ, and the temperature bias over the membrane ΔT ($\Delta T = T_{hot} - T_{cold}$).[45,63] Considering basic permeation principles, thin (small L_x values) aerogel membranes with large A and D_γ should result in higher air conductance within the membrane which should lead to higher air flow rates.[45] The dimensions of the membranes fabricated in the LTCC mold (11 mm × 8 mm × 1 mm) used in this study were 9 × 6 × 0.75 mm^3 (Figure 1a–c). A further reduction of the membrane thickness is possible in terms of feasibility of the fabrication process but would compromise the thermal insulation efficiency of the membrane components.

We estimated the active pumping area (A) from the planar cavity area (~54 mm^2) as shown in Figure 1a–c, and the total channel length (L_x) was defined by the thickness of the membranes which slightly varied from membrane to membrane in the range 0.6–0.73 mm (see Figure 1d and Figure S4). The pore radius D_γ is controlled primarily by the silicic acid precursor concentration in the sol. In terms of the thermomolecular flow generated inside the μ-KP, tailoring the pore radius in the size range of the mean free path of the air molecules is essential and, together with the operating temperature (T_{hot}) and the temperature bias ΔT, limits the air flow rate density.

The maximum attainable ΔT between hot and cold sides of the membrane,[45,63] which is the driving force of the thermal transpiration of gas moleculars, is directly linked to the thermal conductivity λ of the membrane material as well as the maximium operating temperature at the hot-side of the membrane material. In other words, the thermal stability of the membrane material determines the maximum operating temperature at the hot side, as a too high operating temperature would destroy the membrane material or lead to a change in pore morphology, causing rapid performance degradation. For example, a state of the art cellulose membrane has been reported to achieve a ΔT up to 60 °C,[64] but the typical degradation temperature of such a material is well below 300 °C,[65] which, together with the intrinsically high thermal

DOI: 10.1021/acsami.5b05462
ACS Appl. Mater. Interfaces 2015, 7, 18803–18814

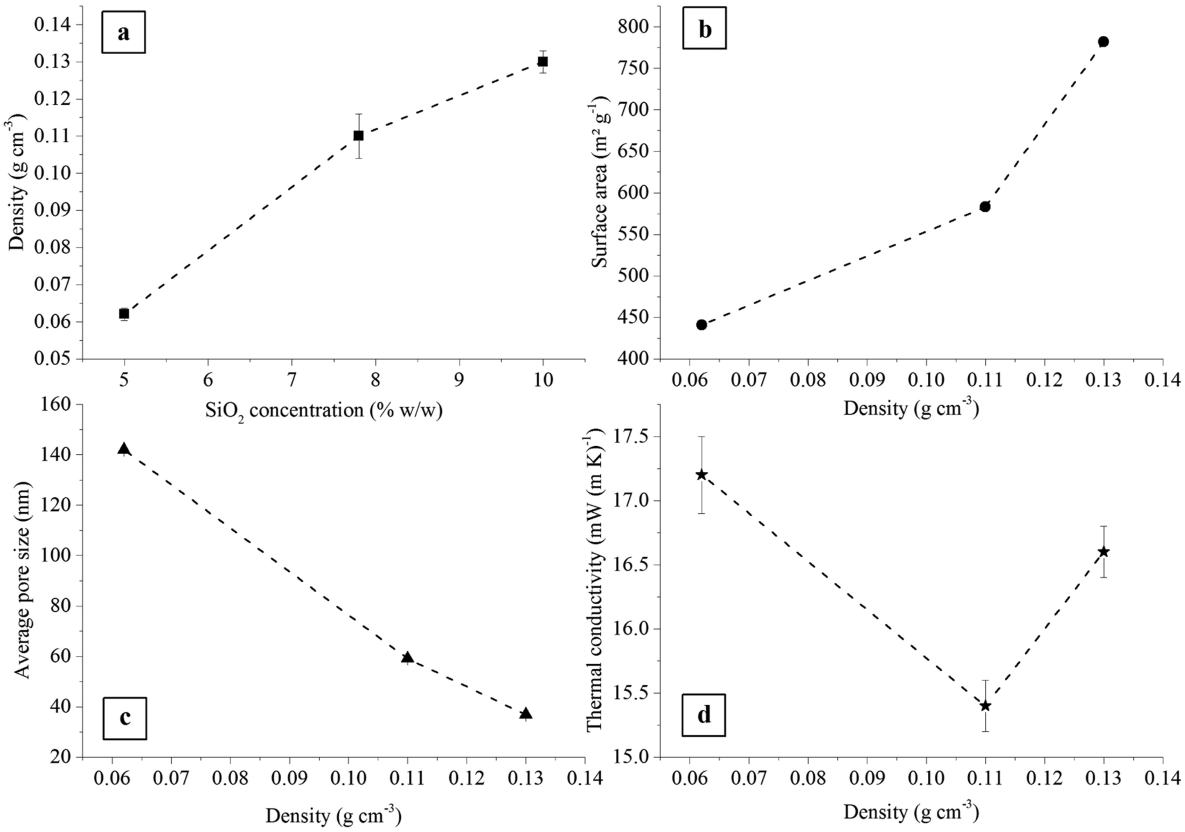

Figure 2. Aerogel membrane materials properties as a function of SiO_2 concentration and envelope density: (a) concentration of the SiO_2 in the sols versus density, (b) density versus specific surface area, (c) density versus average pore size, and (d) density versus thermal conductivity.

conductivity of cellulose limits the application range and the potential for improvement. For silica aerogel membranes, thermogravimetric results (see Figure 1e and Figure S5) suggest that thermal degradation begins around of 420 °C − 440 °C. This is mostly due to the loss of hydrophobic groups (e.g., trimethylsilyl groups) from the silica aerogel backbone (FTIR shown in Figure S6).[66,67] This first generation of silica aerogel membrane μ-KPs can be operated at T_{hot} up to 400 °C, with room for improvement if other, more thermally durable hydrophobization chemistries were to be used. From this point of view, silica-based aerogel membranes offer a key intrinsic advantage of thermal stability over organic- and biopolymer-based analogs, even if similarly low thermal conductivities could be achieved with competing materials.

Not only thermomolecular flow but also the thermal insulating performance of aerogel materials is directly linked to the unique mesoporous structure. Nowadays, silica aerogels are slowly finding their way into markets as high-performance solutions, however most applications are restricted to ambient temperatures. At 23 °C and 50% relative humidity for example (see Figure 2d), the thermal conductivity λ of the identically prepared reference materials are all in the range of super-insulating materials, i.e., below 20×10^{-3} W m^{-1} K^{-1}: SA-7.8-M with a density of 0.11 g cm^{-3} exhibited the lowest λ value of all aerogel materials studied in this work of 15.4×10^{-3} W m^{-1} K^{-1}. Both the lower and higher density samples displayed higher ambient thermal conductivities due to increased gas and radiative transport and skeletal conduction, respectively.[41] At high temperature (T_{hot} = ~400 °C), infrared thermography on the μ-KP setup in operation suggested an effective ΔT between hot and cold membrane sides of approximately 90 °C (shown in Figure S7) corresponding to a mean temperature gradient of 1200K cm^{-1}. Nevertheless, the high-temperature thermal conductivity is dominated by radiative heat transfer. Consequently, the membranes could be further improved by adding infrared opacifiers (such as TiO_2) or absorbers (such as carbon black) to reduce thermal radiation losses.[68] For such thin membranes (≤1 mm), the influence of opacifiers and their spatial distribution on the total thermal conductivity is still unknown and this will be the subject of a follow-up study.

The gas conductance within the membrane is defined to a large extent by the aerogel's pore structure, morphology and hydrophobicity. As previously mentioned, these properties can be engineered by tuning the silica precursor concentration and the specific preparation processes (aging, hydrophobization and drying). The increase of the silica precursor concentration of the sols from 5% to 10% w/w resulted in an increase in bulk density from 0.062 to 0.130 g cm^{-3} (Figure 2a), which corresponds to a decrease in porosity from 97% to 94%. Over this range of density and porosity, the average pore size and μ-KP flow rates varied by a factor of 3.8 and 6.2, respectively, as seen in detail in Table 2.

When designing a thermomolecular pump membrane, the choice of D_γ is essential to ensure that gas moleculars are staying in the transitional flow regime which in turn enables optimal pumping performance.[9,69] Three considerations must be taken account in the determination of the D_γ in the special case of a silica aerogel membrane:

(i) The standard formalism describing KP devices is based on a "classical" thermal transpiration membrane consisting of an array of capillary channels running perpendicular to the membrane surface. Clearly, this is

DOI: 10.1021/acsami.5b05462
ACS Appl. Mater. Interfaces 2015, 7, 18803−18814

Table 2. Comparison of the Flow Rate Density of μ-KP Demonstrators Made from Selected Silica Aerogel Membranes at an Operating Temperature of 400°C

samples	avg. pore size (nm)	surface properties	flow rate density (sccm cm^{-2})
SA-5-M	142.0	hydrophobic	3.85
SA-7.8-M	59.1	hydrophobic	2.72
SA-10-M	36.9	hydrophobic	0.62
SA-5-U	92.6	hydrophilic	0.79

not a good representation of the true structure of a silica aerogel membrane which is made up of randomly distributed pores in a three-dimensional particle-network structure and which is confirmed by the multimodal pore size distribution in the BJH nitrogen sorption data analysis (Figure 3b). Average pore sizes in the aerogel membranes studied in this work span a range between 36.9 and 140 nm.

(ii) Pore sizes of silica aerogel materials obtained from BJH analysis of nitrogen sorption data are often falsely reported with typical values in the 10−20 nm range.[45,70] As described in the literature, BJH results derived from nitrogen sorption data systematically underestimate the pore volume V'_{pore} by a factor of 2 to 3.5 when compared to the V_{pore} derived from the envelope and skeletal density (Table 1). In deformable low-density aerogel materials, this underestimation is due to a structural deformation of the aerogel upon desorption in the capillary condensation range.[41,71] Furthermore, macropores >100 nm are difficult to detect by gas sorption techniques. Given that BJH significantly underestimates the pore volume in aerogels, we adhere to the more meaningful average pore diameter D_{pore} rather than the BJH derived D'_{pore} as a design guide for D_γ.

(iii) The exact operating conditions must be considered when trying to predict the mean free path of the gas. These conditions include temperature, pressure, and the gas type eq 1.[72] Furthermore, the representative l_m and Knudsen number (K_n) have to be calculated under realistic operating conditions (pressure and temperature). In this study, we have calculated *Kn* from the respective pore volume (V_{pore}) and the average pore diameter (D_{pore}) obtained from envelope and skeletal density values. Pore volumes and average pore sizes are linked to the silica concentration in the sol and the final aerogel density (see Figure 2c) and are determined using eqs S3 and S4. D_{pore} (which should correlate with D_γ) is strongly dependent on the silica content: reducing the silica loading from 10 to 5% w/w induces a 3.5 times increase of the average pore size. The mean free path of the air molecules l_m was estimated to 140 nm at an operating temperature of 400 °C for T_{hot}, according to eq 3.

$$l_m = \frac{k_B T_{avg}}{\sqrt{2}\,\pi d_g^2 P} \tag{3}$$

Where k_B is the Boltzmann constant, whose accepted value in SI units is 1.381×10^{-23} J K^{-1}; d_g is the diameter of a gas molecule, which is 3.711×10^{-10} m for nitrogen;[73] T_{avg} is the calculated average temperature in the aerogel membrane, where the hot side is T_{hot} = 400 °C and cold side is T_{cold} = 310 °C; and P is the standard atmospheric pressure (1.013×10^5 Pa).

The value of K_n, calculated from eq 4 and listed in Table 1, ranges from 1.0 (5% w/w silica loading) to 3.8 (10% w/w silica loading). According to the literature, the efficiency of thermal creep (transpiration) is highest for[9,45]

$$K_n = \frac{l_m}{D_\gamma} \tag{4}$$

Where l_m is mean free path of the air molecules derived from eq 3, and D_γ is the characteristic system size, i.e the average pore size of the membrane material.

Nitrogen sorption experiments (BET) were conducted on the aerogel membrane materials to elucidate the pore morphology. The N_2 adsorption−desorption isotherms and pore size distribution of the membrane materials are shown in Figure 3. According to IUPAC classification, the isotherms represent the type IV with a hysteresis loop of type H1 at p/p_0 > 0.45, indicating capillary condensation and evaporation which are typical for mesopores of cylindrical geometry.[56,74] The quantity of N_2 adsorbed at low partial pressures (p/p_0 = 0.1) is due to micropores (shown in Figure 3). As expected, the micropore volumes increase more or less linearly with increasing silica content in the sol, indicating that samples with higher silica constitute more micropores, which simply originate from a higher number density or partially microporous colloidal silica building blocks in the aerogel structure.

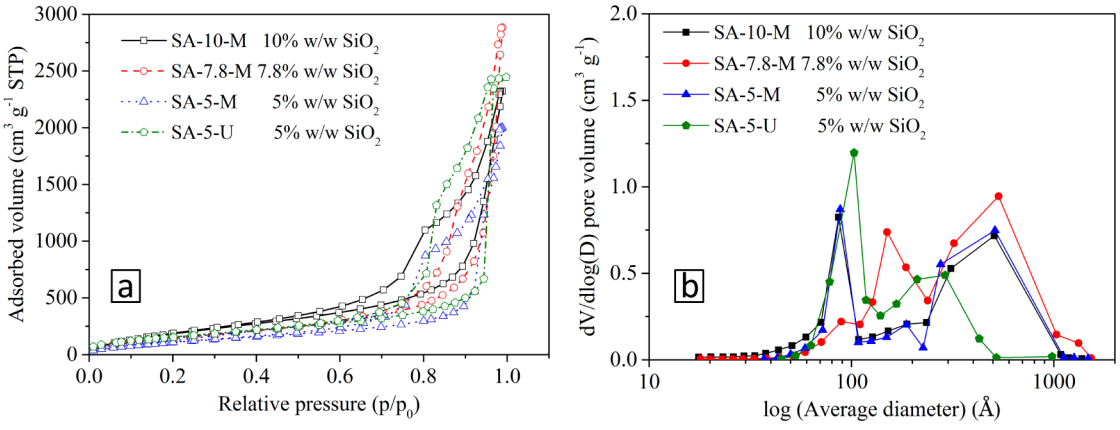

Figure 3. (a) Nitrogen adsorption and desorption isotherms and (b) BJH pore size distribution for silica aerogel materials used for fabricating membranes.

DOI: 10.1021/acsami.5b05462
ACS Appl. Mater. Interfaces 2015, 7, 18803−18814

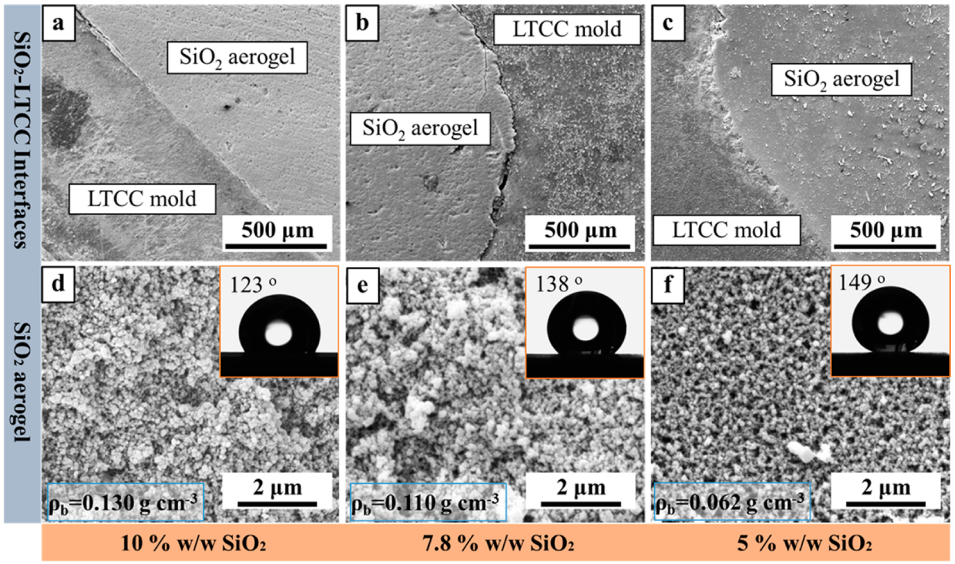

Figure 4. SEM images of interface between (a–c) SiO_2 aerogel and LTCC mold and (d–f) SiO_2 aerogel membranes.

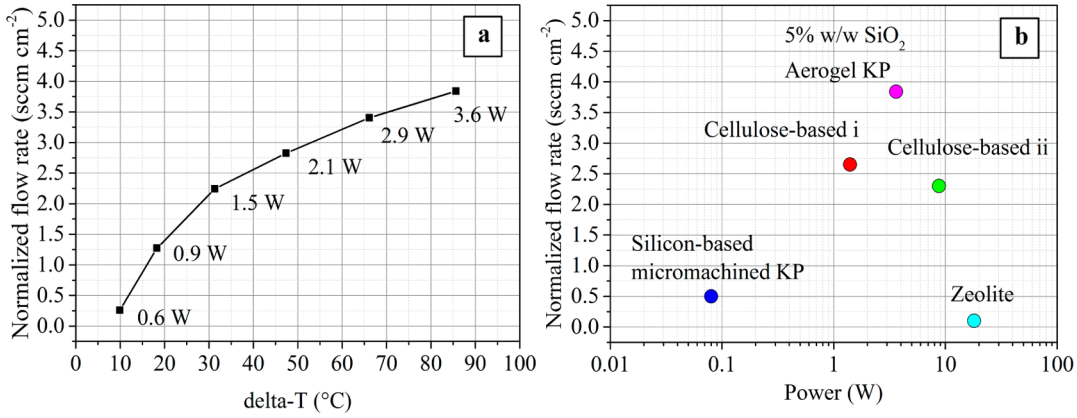

Figure 5. (a) Normalized flow rate versus operating temperature (and power consumption) in a μ-KP demonstrator using an aerogel membrane with 5% w/w SiO_2, (b) benchmark (collected data from the literature[7564]) of μ-KP gas pump system assembled with as-prepared aerogel membranes.

As is typical for silica aerogels, the amount N_2 adsorbed around a partial pressure of 0.1 of all samples is only around 5–10% of the total uptake, confirming that micropores are a minority species. The largest uptake is in the range from 0.10 to 0.95 (p/p_0), indicating a majority of mesopores. Higher silica sol concentrations (aerogel densities) lead to a more narrow, mechanical deformation induced hysteresis loop (SA-7.8-M and SA-10-M are narrower than SA-5-M and SA-5-U). The mechanical deformation is due to a springback-type effect which occurs during wet gel "drying" upon liquid N_2 desorption. Although the width and area under the hysteresis loop in the capillary condensation range is linked to mechanical properties, a more detailed understanding of this phenomenon is still lacking. The pore size distribution obtained from BJH analysis is presented in (Figure 3b), showing a broad, bimodal distribution.

The replication quality of the aerogel membrane/LTCC mold assemblies were examined in detail using SEM microscopy as shown in Figure 4. All aerogel membranes are perfectly integrated inside the LTCC molds with a good shape replication and contour fidelity. Upon higher resolution inspection, the aerogels display the typical mesoporous three-dimensional network structure (Figure 4d–f). Interfacial gaps or cracks between the LTCC mold and the membrane are nonexistent or barely visible and no additional disjoining was found even after hours of operation inside the μ-KP demonstrator. Although typically 2–5% of linear shrinkage is assumed as a practically achievable minimal shrinkage value for larger monolithic low-density aerogel materials over the entire production history, SEM results confirmed that our optimized procedure yielded close-to-ideal, reproducible production of high-quality aerogel membranes with virtually zero shrinkage (estimated around 0.3% from dimension analysis): the small cracks between the membrane and LTCC in SA-7.8-M are less than 10 μm wide and hence cause a hydrodynamic short of the effective membrane area (see Figure 1a–c, effective area starts ~50 μm from the boundary). In conclusion, monolithic crack-free membranes with tunable structural morphology in full conformity with the design specifications could be obtained by the mold casting method from silicic acid sols. In agreement with BET results, SA-5-M (D_{pore} of 142 nm, shown in Table 1) displays a quite homogeneous distribution of macropores and smaller secondary particles, whereas SA-7.8-M and SA-10-M

DOI: 10.1021/acsami.5b05462
ACS Appl. Mater. Interfaces 2015, 7, 18803–18814

display larger secondary particles featuring significantly smaller pores in the upper mesoporous range.

Performance and Application Potential of Miniaturized Knudsen Gas Pumps. In this section air pumping performance measurements using a MEMS type μ-KP prototype built from in-house developed silica aerogel membranes as active components are described. The operating temperature of the device, corresponding to T_{hot}, was defined as the temperature of the integrated platinum heating element which was simultaneously used as a temperature probe (in situ resistivity measurement). The test setup was designed for regulating the operating temperature and measuring the flow rate simultaneously and was calibrated prior to μ-KP test runs. The details of the testing setup as well as the development of the μ-KPs will be discussed in a follow-up article. Video S1 shows the air pumping performance of the complete μ-KP setup at T_{hot} = 400 °C and ΔT = 90 °C.

Figure 5a shows the pumping performance with the increasing operating temperature in terms of normalized flow rate density, which is defined as the flow rate per unit area of the aerogel membrane. It was found that the SA-5-M membrane was able to deliver 3.85 sccm cm^{-2} of air flow at the operating temperature of 400 °C and a bias of 90 °C (see Figure 5a). With increasing temperature bias across the aerogel membrane, a higher flow rate was recorded as shown in Figure 5a.[9,59] It was also found that the larger pore size aerogel membranes resulted in improved pumping efficiency: the aerogel membrane with 5% w/w SiO_2 loading achieved significantly higher flow rate than others with 10% or 7.8% w/w SiO_2 (see Table 2), indicating that over a certain range, larger pore sizes improve the gas conductance. Generally speaking, larger-sized pores in the aerogel membrane lead to larger hydraulic diameters of the flow-channels and consequently to smaller Knudsen numbers. This causes the air transport mechanism to move more into the viscous flow regime. As flow rate and maximum operating pressure difference are linked, it is expected that a reduction of flow rate comes with higher dynamic backpressures of the device during operation. Characterization of the μ-KP pressure dependent flow-rates will be the focus of a future study. From the literature it has been suggested that a μ-KP is able to achieve optimal performance within the transition flow regime ($0.1 < K_n < 10$). For the aerogel membranes prepared in this study, the corresponding Knudsen numbers range from 1.0 to 3.8 under the given pressure and temperature conditions, indicating that the membranes operate in the transition flow regime, which is experimentally confirmed by the high device performance.

For a miniaturized air pump, the power consumption and its relationship with the pumping performance is critical, particularly to point out opportunities for continuing device development. By comparison with other literature works, we found that our silica aerogel membrane based μ-KP was able to deliver pumping rates up to of 3.85 sccm cm^{-2} at a power consumption of 3.6 W (see Figure 5b). This performance is about 50% higher than comparable pumps based on cellulose membranes of similar power output. We attribute the outstanding performance of silica aerogel membrane μ-KPs to the low thermal conductivity of the aerogel material and its high thermal stability. An additional advantage is the relatively easy structure control of the gel synthesis which allows facile custom tailoring of the membranes to suit specific needs. By combining very low thermal conductivity and high thermal stability, aerogel membranes can build up a larger temperature gradient resulting in sizable thermal transpiration driven pressure differences. Control of the pore sizes in the meso- and macroporous range boasts gas conductance which allows for more efficient thermomolecular pumping.

In addition, the surface chemistry of the silica aerogel membrane is a critical parameter for optimal μ-KP pumping performance: compared to the hydrophobic samples (SA-5-M), samples with the same silica loading and hydrophilic surface chemistry showed an almost 5-fold lower air flow rate density under the same testing conditions (0.79 sccm cm^{-2} vs 3.85 sccm cm^{-2}, see Table 2). Contact angle measurements confirmed the hydrophobic nature of the silylated aerogel membranes, displaying very high water contact angles (see Figure 4 insets). The water contact angle of SA-5-U was close to 0° but could not be experimentally measured, as the water droplet was immediately absorbed by the nonhydrophobized aerogel which resulted in the immediate collapse of the aerogel structure. Post-mortem analysis of hydropholic membranes suggests that the low pumping performance of such aerogel membranes is due to their strong interaction with water vapor during operation: the water vapor easily adsorbs onto the pore surfaces causing structural changes and damage in the pore structure which impedes normal thermal transpiration operation.

CONCLUSIONS

We have successfully developed a novel and simple sol−gel process for manufacturing silica aerogel membranes and demonstrated their outstanding performance in MEMS based miniaturized thermomolecular pump prototypes. Using such a process, hydrophobic silica aerogel membranes with tunable pore size can be easily fabricated within an LTCC mold by gel casting. These membranes were then readily integrated into a customized μ-KP test demonstrator. The flexibility of the membrane fabrication processing has allowed us to study the correlation between the pore structure of the materials and the pumping performance of μ-KP systems. Normalized flow rate densities as high as of 3.85 sccm cm^{-2} using a hydrophobic silica aerogel membrane with an average pore size of 142 nm were measured in the μ-KP test stand at an operating temperature of 400 °C (hot side) and a temperature bias of 90 °C. This type of membrane currently holds the record for highest air pumping performance in a single stage KP benchmark reported so far. This study demonstrates the potential for further development of silica aerogel based high performance miniaturized thermal transpiration air pumps for microsystems applications. Such a technology is expected to advance miniaturized energy conversion and sensing devices, provided that the fundamentals of molecular pumping in three-dimensional open-mesoporous materials is better understood and described by improved theoretical models.

ASSOCIATED CONTENT

Supporting Information

The Supporting Information is available free of charge on the ACS Publications website at DOI: 10.1021/acsami.5b05462.

Additional information and Figures S1−S7 (PDF)

Video S1 (ZIP)

DOI: 10.1021/acsami.5b05462
ACS Appl. Mater. Interfaces 2015, 7, 18803−18814

AUTHOR INFORMATION

Corresponding Authors

*E-mail: bo.jiang@alumni.epfl.ch.
*E-mail: matthias.koebel@empa.ch.

Author Contributions

The manuscript was written through contributions of all authors. All authors have given approval to the final version of the manuscript.

Notes

The authors declare no competing financial interest.

ACKNOWLEDGMENTS

This work is part of the project on "Aerogels from sodium silicate—towards cost-effective mass production technologies" (BFE, contract SI/500777-01) and is financed by the Bundesamt für Energie and Swiss National Science Foundation (contract 200021_143424). Thanks to Beatrice Fischer for her assistance with the TGA measurements and Stefanie Hauser for the help with the supercritical CO_2 drying. The authors appreciate Dr. Wim Malfait for his discussion and revision. The authors also thank the Swiss National Science Foundation for funding ASAP2020c equipment within the R'Equip program (project 206021_128741/1).

ABBREVIATIONS

MEMS, microeletromechanical systems
μ-KPs, micro-Knudsen pumps
LTCC, Low-temperature co-fired ceramic technology
PS, polystyrene
TEOS, tetraethyl orthosilicate
WCAs, water contact angles
BET, nitrogen sorption experiments
BJH, Barrett—Joyner—Halender

REFERENCES

(1) Qin, D.; Xia, Y.; Rogers, J.; Jackman, R.; Zhao, X.-M.; Whitesides, G. Microfabrication, Microstructures and Microsystems. In *Microsystem Technology in Chemistry and Life Science*; Manz, A., Becker, H., Eds.; Springer: Berlin, 1998; Chapter 1, pp 1—20.
(2) Ohira, S. I.; Toda, K. Micro Gas Analysis System for Measurement of Atmospheric Hydrogen Sulfide and Sulfur Dioxide. *Lab Chip* **2005**, *5* (12), 1374—1379.
(3) Malzbender, J.; Steinbrech, R.; Singheiser, L. A Review of Advanced Techniques for Characterising SOFC Behaviour. *Fuel Cells* **2009**, *9* (6), 785—793.
(4) Bieberle-Hütter, A.; Beckel, D.; Infortuna, A.; Muecke, U. P.; Rupp, J. L.; Gauckler, L. J.; Rey-Mermet, S.; Muralt, P.; Bieri, N. R.; Hotz, N.; et al. A Micro-Solid Oxide Fuel Cell System as Battery Replacement. *J. Power Sources* **2008**, *177* (1), 123—130.
(5) Dyer, C. K. Fuel Cells for Portable Applications. *J. Power Sources* **2002**, *106* (1—2), 31—34.
(6) Segal, A.; Górecki, T.; Mussche, P.; Lips, J.; Pawliszyn, J. Development of Membrane Extraction with a Sorbent Interface—Micro Gas Chromatography System for Field Analysis. *J. Chromatogr. A* **2000**, *873* (1), 13—27.
(7) Knudsen, M. Eine Revision der Gleichgewichtsbedingung der Gase. Thermische Molekularströmung. *Ann. Phys. (Berlin, Ger.)* **1909**, *336* (1), 205—229.
(8) Knudsen, M. Thermischer Molekulardruck der Gase in Röhren. *Ann. Phys. (Berlin, Ger.)* **1910**, *338* (16), 1435—1448.
(9) Vargo, S.; Muntz, E.; Shiflett, G.; Tang, W. Knudsen Compressor as a Micro-and Macroscale Vacuum Pump Without Moving Parts or Fluids. *J. Vac. Sci. Technol., A* **1999**, *17* (4), 2308—2313.
(10) Young, M.; Han, Y.; Muntz, E.; Shiflett, G. Characterization and Optimization of a Radiantly Driven Multi-stage Knudsen Compressor. In *Rarefied Gas Dynamics: 24th International Symposium on Rarefied Gas Dynamics*; Monopoli, Italy, July 10—16, 2004 ; American Institute of Physics: College Park, MD, 2005.
(11) Han, Y.-L.; Muntz, E. Experimental Investigation of Micro-Mesoscale Knudsen Compressor Performance at Low Pressures. *J. Vac. Sci. Technol., B: Microelectron. Nanometer Struct.–Process., Meas., Phenom.* **2007**, *25* (3), 703—714.
(12) Muntz, E.; Sone, Y.; Aoki, K.; Vargo, S.; Young, M. Performance Analysis and Optimization Considerations for a Knudsen Compressor in Transitional Flow. *J. Vac. Sci. Technol., A* **2002**, *20* (1), 214—224.
(13) Vargo, S.; Muntz, E.; Shiflett, G.; Tang, W. Knudsen Compressor as a Micro-and Macroscale Vacuum Pump Without Moving Parts or Fluids. *J. Vac. Sci. Technol., A* **1999**, *17* (4), 2308—2313.
(14) Gupta, N. K.; Masters, N. D.; Ye, W.; Gianchandani, Y. B. Gas Flowin Nano-Channels: Thermal Transpirationmodelswith Application to a Si-Micromachinedknudsen Pump. In *TRANSDUCERS 2007: International Solid-State Sensors, Actuators and Microsystems Conference*; IEEE: Piscataway, NJ, 2007; pp 2329—2332.
(15) Ohwada, T.; Sone, Y.; Aoki, K. Numerical Analysis of the Poiseuille and Thermal Transpiration Flows Between Two Parallel Plates on the Basis of the Boltzmann Equation for Hard-Sphere Molecules. *Phys. Fluids A* **1989**, *1*, 2042.
(16) Copic, D.; McNamara, S. Efficiency Derivation for the Knudsen Pump with and Without Thermal Losses. *J. Vac. Sci. Technol., A* **2009**, *27* (3), 496—502.
(17) Reim, M.; Korner, W.; Manara, J.; Korder, S.; Arduini Schuster, M.; Ebert, H. P.; Fricke, J. Silica Aerogel Granulate Material for Thermal Insulation and Daylighting. *Sol. Energy* **2005**, *79* (2), 131—139.
(18) Neumann, P.; Rohrmann, T. Lattice Boltzmann Simulations in the Slip and Transition Flow Regime with the Peano Framework. *Open J. Fluid Dyn.* **2012**, *2* (3), 101—110.
(19) Lu, X.; Wang, P.; Buttner, D.; Heinemann, U.; Nilsson, O.; Kuhn, J.; Fricke, J. Thermal Transport in Opacified Monolithic Silica Aerogels. *High Temp.—High Pressure* **1991**, *23* (4), 431—436.
(20) Hæreid, S.; Nilsen, E.; Einarsrud, M. A. Subcritical Drying of Silica Gels. *J. Porous Mater.* **1995**, *2* (4), 315—324.
(21) Rao, A. V.; Wagh, P. B. Preparation and Characterization of Hydrophobic Silica Aerogels. *Mater. Chem. Phys.* **1998**, *53* (1), 13—18.
(22) Schmidt, M.; Schwertfeger, F. Applications for Silica Aerogel Products. *J. Non-Cryst. Solids* **1998**, *225* (1), 364—368.
(23) Smith, D. M.; Maskara, A.; Boes, U. Aerogel-Based Thermal Insulation. *J. Non-Cryst. Solids* **1998**, *225* (0), 254—259.
(24) Ehrburger-Dolle, F.; Dallamano, J.; Elaloui, E.; Pajonk, G. M. Relations Between the Texture of Silica Aerogels and Their Preparation. *J. Non-Cryst. Solids* **1995**, *186* (0), 9—17.
(25) Job, N.; Thery, A.; Pirard, R.; Marien, J.; Kocon, L.; Rouzaud, J.-N.; Beguin, F.; Pirard, J.-P. Carbon Aerogels, Cryogels and Xerogels: Influence of the Drying Method on the Textural Properties of Porous Carbon Materials. *Carbon* **2005**, *43* (12), 2481—2494.
(26) Kawashima, D.; Aihara, T.; Kobayashi, Y.; Kyotani, T.; Tomita, A. Preparation of Mesoporous Carbon from Organic Polymer/Silica Nanocomposite. *Chem. Mater.* **2000**, *12* (11), 3397—3401.
(27) Kyotani, T. Control of Pore Structure in Carbon. *Carbon* **2000**, *38* (2), 269—286.
(28) Yamamoto, T.; Sugimoto, T.; Suzuki, T.; Mukai, S. R.; Tamon, H. Preparation and Characterization of Carbon Cryogel Microspheres. *Carbon* **2002**, *40* (8), 1345—1351.
(29) Tamon, H.; Ishizaka, H. Preparation of Organic Mesoporous Gel by Supercritical/Freeze Drying. *Drying Technol.* **1999**, *17* (7—8), 1653—1665.
(30) Rudaz, C.; Courson, R.; Bonnet, L.; Calas-Etienne, S.; Sallée, H.; Budtova, T. Aeropectin: Fully Biomass-Based Mechanically Strong and Thermal Superinsulating Aerogel. *Biomacromolecules* **2014**, *15* (6), 2188—2195.

DOI: 10.1021/acsami.5b05462
ACS Appl. Mater. Interfaces 2015, 7, 18803—18814

(31) Zhao, S.; Zhang, Z.; Sèbe, G.; Wu, R.; Rivera Virtudazo, R. V.; Tingaut, P.; Koebel, M. M. Multiscale Assembly of Superinsulating Silica Aerogels Within Silylated Nanocellulosic Scaffolds: Improved Mechanical Properties Promoted by Nanoscale Chemical Compatibilization. *Adv. Funct. Mater.* **2015**, *25* (15), 2326−2334.
(32) Hammouda, L.; Mejri, I.; Younes, M.; Ghorbel, A. ZrO_2 Aerogels. In *Aerogels Handbook*; Aegerter, M. A., Leventis, N., Koebel, M. M., Eds.; Springer: New York, 2011; Chapter 6, pp 127−143.
(33) Hirashima, H. Preparation of TiO_2 Aerogels-Like Materials Under Ambient Pressure. In *Aerogels Handbook*; Aegerter, M. A., Leventis, N., Koebel, M. M., Eds.; Springer: New York, 2011; Chapter 7, pp 145−153.
(34) Fesmire, J. E. Aerogel Insulation Systems for Space Launch Applications. *Cryogenics* **2006**, *46* (2−3), 111−117.
(35) Poco, J. F.; Coronado, P. R.; Pekala, R. W.; Hrubesh, L. W.; Beck, J.S.; C, D. R.; Davis, M.E.; Iton, L.E.; Lobo, R.F. Rapid Supercritical Extraction Process for the Production of Silica Aerogels. *MRS Proc.* **1996**, *431*, 297−302.
(36) Lee, S.; Lee, E. A.; Hwang, H. J.; Moon, J. W.; Han, I. S.; Woo, S.-K. Solvents Effects on Physicochemical Properties of Nano-Porous Silica Aerogels Prepared by Ambient Pressure Drying Method. In *Materials Science Forum*; Trans Tech: Stafa-Zurich, Switzerland, 2006; Vols. *510*−*511*, pp 910−913.
(37) Dutoit, D. C. M.; Schneider, M.; Baiker, A. Titania-Silica Mixed Oxides: I. Influence of Sol-Gel and Drying Conditions on Structural Properties. *J. Catal.* **1995**, *153* (1), 165−176.
(38) Feng, J.; Chen, D.; Ni, W.; Yang, S.; Hu, Z. Study of IR Absorption Properties of Fumed Silica-Opacifier Composites. *J. Non-Cryst. Solids* **2010**, *356* (9−10), 480−483.
(39) Potter, R. M.; Gavin, P. M.; Grieco, W. J.; Choudhary, M. K. High Thermal Resistivity Insulation Material with Opacifier Uniformly Distributed Thoughout. US 20120251796 A1, 2012.
(40) Caps, R.; Fricke, J. Thermal Conductivity of Opacified Powder Filler Materials for Vacuum Insulations. *Int. J. Thermophys.* **2000**, *21* (2), 445−452.
(41) Wong, J. C. H.; Kaymak, H.; Brunner, S.; Koebel, M. M. Mechanical Properties of Monolithic Silica Aerogels Made from Polyethoxydisiloxanes. *Microporous Mesoporous Mater.* **2014**, *183* (0), 23−29.
(42) Venkateswara Rao, A.; Nilsen, E.; Einarsrud, M. A. Effect of Precursors, Methylation Agents and Solvents on the Physicochemical Properties of Silica Aerogels Prepared by Atmospheric Pressure Drying Method. *J. Non-Cryst. Solids* **2001**, *296* (3), 165−171.
(43) Rao, A. P.; Rao, A. V.; Pajonk, G. M. Hydrophobic and Physical Properties of the Ambient Pressure Dried Silica Aerogels with Sodium Silicate Precursor Using Various Surface Modification Agents. *Appl. Surf. Sci.* **2007**, *253* (14), 6032−6040.
(44) Nyquist, R. A.; Kagel, R. O. Preface. In *Handbook of Infrared and Raman Spectra of Inorganic Compounds and Organic Salts*; Nyquist, R. A., Kagel, R. O., Eds.; Academic Press: San Diego, 1971; p vii.
(45) Han, Y.-L.; Muntz, E. Experimental Investigation of Micro-Mesoscale Knudsen Compressor Performance at Low Pressures. *J. Vac. Sci. Technol., B: Microelectron. Nanometer Struct.–Process., Meas., Phenom.* **2007**, *25* (3), 703−714.
(46) Han, Y. J.; Watson, J. T.; Stucky, G. D.; Butler, A. Catalytic Activity of Mesoporous Silicate-Immobilized Chloroperoxidase. *J. Mol. Catal. B: Enzym.* **2002**, *17* (1), 1−8.
(47) Ochoa, F.; Ronney, P. D. A Thermal Transpiration-Based Self-Pressurizing Mesoscale Combustor. In *Proceedings of the 6th International Workshop on Micro and Nanotechnology for Power Generation and Energy Conversion Applications*; Berkeley, CA, Nov 29−Dec 1, 2006 ; Frechette, L. G., Ed..
(48) Venkateswara Rao, A.; Bhagat, S. D. Synthesis and Physical Properties of TEOS-Based Silica Aerogels Prepared by Two Step (Acid-Base) Sol-Gel Process. *Solid State Sci.* **2004**, *6* (9), 945−952.
(49) Hwang, S.-W.; Jung, H.-H.; Hyun, S.-H.; Ahn, Y.-S. Effective Preparation of Crack-Free Silica Aerogels via Ambient Drying. *J. Sol-Gel Sci. Technol.* **2007**, *41* (2), 139−146.
(50) Judeinstein, P.; Titman, J.; Stamm, M.; Schmidt, H. Investigation of Ion-Conducting Ormolytes: Structure-Property Relationships. *Chem. Mater.* **1994**, *6* (2), 127−134.
(51) Lee, C. J.; Kim, G. S.; Hyun, S. H. Synthesis of Silica Aerogels from Waterglass via New Modified Ambient Drying. *J. Mater. Sci.* **2002**, *37* (11), 2237−2241.
(52) Shi, F.; Wang, L.; Liu, J. Synthesis and Characterization of Silica Aerogels by a Novel Fast Ambient Pressure Drying Process. *Mater. Lett.* **2006**, *60* (29−30), 3718−3722.
(53) Sun, J.; Longtin, J. P.; Norris, P. M. Ultrafast Laser Micromachining of Silica Aerogels. *J. Non-Cryst. Solids* **2001**, *281* (1−3), 39−47.
(54) Jiang, B.; Muralt, P.; Maeder, T. Meso-Scale Ceramic Hotplates − A Playground for High Temperature Microsystems. *Sens. Actuators, B* **2015**, *221*, 823−834.
(55) Jiang, B.; Haber, J.; Renken, A.; Muralt, P.; Kiwi-Minsker, L.; Maeder, T. Fine Structuration of Low-Temperature Co-Fired Ceramic (LTCC) Microreactors. *Lab Chip* **2015**, *15* (2), 563−574.
(56) Santhosh Kumar, M.; Hammer, N.; Rønning, M.; Holmen, A.; Chen, D.; Walmsley, J. C.; Øye, G. The Nature of Active Chromium Species in Cr-Catalysts for Dehydrogenation of Propane: New Insights by a Comprehensive Spectroscopic Study. *J. Catal.* **2009**, *261* (1), 116−128.
(57) Stahl, T.; Brunner, S.; Zimmermann, M.; Ghazi Wakili, K. Thermo-Hygric Properties of a Newly Developed Aerogel Based Insulation Rendering for Both Exterior and Interior Applications. *Energy Buildings* **2012**, *44* (0), 114−117.
(58) Rangarajana, B.; Lira, C. T.; Hampden-Smith, M. J.; Klemperer, W. G.; Brinker, C. J. Interpretation of Aerogel Shrinkage during Drying. *MRS Proc.* **1992**, *271*, 559−566.
(59) Yen-Lin, H. Thermal-Creep-Driven Flows in Knudsen Compressors and Related Nano/Microscale Gas Transport Channels. *J. Microelectromech. Syst.* **2008**, *17* (4), 984−997.
(60) Pierre, A.; Rigacci, A. SiO_2 Aerogels. In *Aerogels Handbook*; Aegerter, M. A., Leventis, N., Koebel, M. M., Eds.; Springer: New York, 2011; Chapter 2, pp 21−45.
(61) Venkateswara Rao, A.; Nilsen, E.; Einarsrud, M. A. Effect of Precursors, Methylation Agents and Solvents on the Physicochemical Properties of Silica Aerogels Prepared by Atmospheric Pressure Drying Method. *J. Non-Cryst. Solids* **2001**, *296* (3), 165−171.
(62) van Bommel, M. J.; de Haan, A. B. Drying of Silica Aerogel with Supercritical Carbon Dioxide. *J. Non-Cryst. Solids* **1995**, *186*, 78−82.
(63) Gupta, N. K.; Gianchandani, Y. B. Thermal Transpiration in Zeolites: a Mechanism for Motionless Gas Pumps. *Appl. Phys. Lett.* **2008**, *93* (19), 193511−193511−3.
(64) Pharas, K.; McNamara, S. Knudsen Pump Driven by a Thermoelectric Material. *J. Micromech. Microeng.* **2010**, *20* (12), 125032.
(65) Madorsky, S. L.; Hart, V. E.; Straus, S. Thermal Degradation of Cellulose Materials. *J. Res. Natl. Bur. Stand. (U. S.)* **1958**, *60* (4), 343−349.
(66) Lee, S.; Cha, Y. C.; Hwang, H. J.; Moon, J.-W.; Han, I. S. The Effect of pH on the Physicochemical Properties of Silica Aerogels Prepared by an Ambient Pressure Drying Method. *Mater. Lett.* **2007**, *61* (14−15), 3130−3133.
(67) Wang, L.; Zhao, S. Synthesis and Characteristics of Mesoporous Silica Aerogels with One-Step Solvent Exchange/Surface Modification. *J. Wuhan Univ. Technol., Mater. Sci. Ed.* **2009**, *24* (4), 613−618.
(68) Xie, T.; He, Y.-L.; Hu, Z.-J. Theoretical Study on Thermal Conductivities of Silica Aerogel Composite Insulating Material. *Int. J. Heat Mass Transfer* **2013**, *58* (1−2), 540−552.
(69) Muntz, E.; Sone, Y.; Aoki, K.; Vargo, S.; Young, M. Performance Analysis and Optimization Considerations for a Knudsen Compressor in Transitional Flow. *J. Vac. Sci. Technol., A* **2002**, *20* (1), 214−224.
(70) Ochoa, F.; Eastwood, C.; Ronney, P.; Dunn, B. Thermal Transpiration Based Microscale Propulsion and Power Generation Devices. In *Proceedings of the 7th International Workshop on Microgravity Combustion and Chemically Reacting Systems*; Cleveland,

DOI: 10.1021/acsami.5b05462
ACS Appl. Mater. Interfaces 2015, 7, 18803−18814

OH, June 3−6, 2003 ; Glenn, J. H., Ed.; NASA Center for Aerospace Information: Hanover, MD, 2003; NASA/CP-2003-21376.
(71) Reichenauer, G. Structural Characterization of Aerogels. In *Aerogels Handbook*; Aegerter, M. A., Leventis, N., Koebel, M. M., Eds.; Springer: New York, 2011; Chapter 21, pp 449−498.
(72) Zeng, S. Q.; Hunt, A.; Greif, R. Transport Properties of Gas in Silica Aerogel. *J. Non-Cryst. Solids* **1995**, *186* (0), 264−270.
(73) Sone, Y. Boltzmann Equation. In *Molecular Gas Dynamics Theory, Techniques, and Applications*; Sone, Y., Ed.; Birkhäuser: Boston, 2007; Chapter 1, pp 1−27.
(74) Groen, J. C.; Peffer, L. A. A.; Pérez-Ramírez, J. Pore Size Determination in Modified Micro- and Mesoporous Materials. Pitfalls and Limitations in Gas Adsorption Data Analysis. *Microporous Mesoporous Mater.* **2003**, *60* (1−3), 1−17.
(75) Gupta, N. K.; Gianchandani, Y. B. Porous Ceramics for Multistage Knudsen Micropumps—Modeling Approach and Experimental Evaluation. *J. Micromech. Microeng.* **2011**, *21* (9), 095029.

DOI: 10.1021/acsami.5b05462
ACS Appl. Mater. Interfaces 2015, 7, 18803−18814